Analyzing the bi-directional dynamic morphing of a bi-stable water-bomb base origami

Sahand Sadeghi, Suyi Li

Sahand Sadeghi, Suyi Li, "Analyzing the bi-directional dynamic morphing of a bi-stable water-bomb base origami," Proc. SPIE 10968, Behavior and Mechanics of Multifunctional Materials XIII, 109680S (29 March 2019); doi: 10.1117/12.2512301

SPIE.

Event: SPIE Smart Structures + Nondestructive Evaluation, 2019, Denver, Colorado, United States

Analyzing the bi-directional dynamic morphing of a bi-stable water-bomb base origami

Sahand Sadeghi* and Suyi Li
Department of Mechanical Engineering, Clemson University, Clemson, SC 29634, USA

ABSTRACT

Morphing structures have been a subject of much research recently because of their promising potentials in aerospace, wind turbine, and many other applications. There exists many different approaches to achieve shape morphing, among which the origami-inspired folding is particularly interesting in that folding is fundamentally three-dimensional, scalable, and customizable. However, activating and attaining large amplitude folding autonomously are challenging. Active materials, such as shape memory alloys, have been used to activate folding, but they are limited due to the power supply requirement to maintain the folded configurations. One possible solution is to embed bi-stability into the origami structure. Bi-stability can play two significant roles: First, it can significantly reduce the actuation requirement to induce shape morning; and second, it can maintain the shape change without demanding sustained energy supply. In this study, we demonstrate the feasibility of using dynamic excitation to induce shape morphing (or folding) between the two stable states of water-bomb base. For the first time, we derive the dynamic equation of motion for a water-bomb base origami and use it extensively to analyze its time responses under harmonic excitation. Via numerical simulations, we show that by harnessing the intra-well resonance of the water-bomb structure, we can achieve rapid bi-directional morphing using relatively low actuation magnitudes in comparison with quasi-static loading.

Keywords: Shape morphing, Origami, Water-bomb base, Bi-stable dynamics, Non-linear dynamics

1. INTRODUCTION

Morphing structures can undergo significant shape reconfigurations to achieve optimal performance according to different operating conditions[1], endowing them with tremendous potentials in aerospace and many other applications[2,3]. For example, many recent achievements and progresses in the aircraft industry have been inspired by the avian morphology observed in nature[4]. That is, birds that can rapidly change the shape of their wings to transition from efficient cruise to aggressive maneuvering and precision descents[2]. In addition, morphing structures have found useful applications in the wind turbine blade implementations because of their capabilities to increase aerodynamic efficiency and lower weight without incurring heavy penalties in construction complexity[5].

Among the various means of achieving shape morphing, origami-inspired folding is particularly advantageous. This is because folding is a powerful approach to induce three-dimensional and sophisticated shape changes; in addition, the principle of folding is geometric and scale-independent. These merits have turned origami folding techniques into a new paradigm for designing multi-functional architected materials and structures[6] with lots of unique properties, e.g. auxetic properties[7], tunable nonlinear stiffness[8] and desired dynamic characteristics[9,10]. However, attaining large amplitude and autonomous folding is still a challenge in origami engineering[11].

Recently, there have been several studies on using active materials to activate folding, such as dielectric elastomers (DE), magneto-active elastomers (MAE) and shape memory alloys (SMA)[12,13]. While promising, the use of these active materials is limited due to the constant energy supply that is required to keep the structure in the desired configuration. One possible solution is to embed bi-stability into the structure. Here, bi-stability can play two significant roles: first, it can significantly reduce the actuation requirement to induce shape morning; and second, it can maintain the shape change without demanding sustained energy supply[11].

* Corresponding author: ssadegh@clemson.edu

Behavior and Mechanics of Multifunctional Materials XIII, edited by Hani E. Naguib, Proc. of SPIE
Vol. 10968, 109680S · © 2019 SPIE · CCC code: 0277-786X/19/$18 · doi: 10.1117/12.2512301

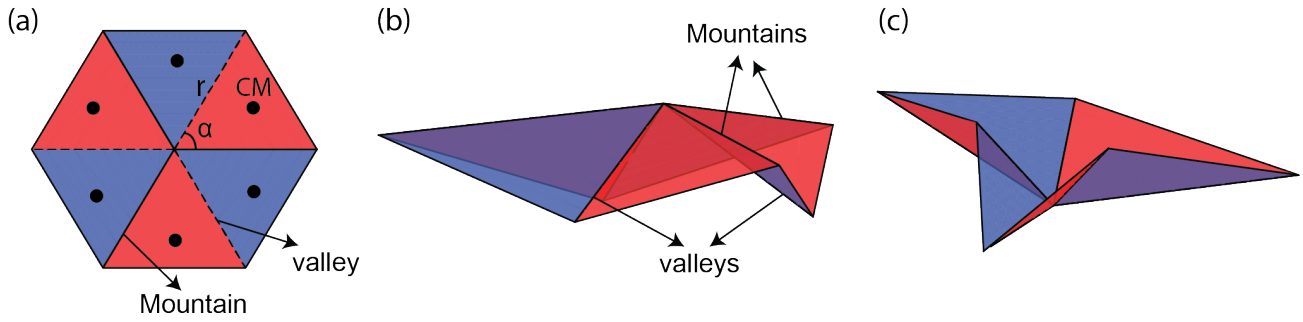

Figure 1. A water-bomb base folding pattern (a), and its first and second stable states, respectively (b, c). The black dots show the location of center of mass (CM) of each facet.

Water-bomb base is a well-known bi-stable origami pattern (Figure 1(a)). Hanna et al. investigated the bi-stable behavior of the water-bomb base using potential energy analysis and experimental validations[14]. In another study, Bowen et al. developed an ADAMS model to capture the bi-stabile behaviors of water bomb base[15], and examined the use of MAE actuators to achieve self-folding. The results of these two studies indicate that, to achieve shape morphing via bi-stability, the actuator needs to force the water-bomb from one stable equilibrium to the critical unstable equilibrium to trigger a "snap-through" response[14,15], but this process could require a relatively large actuation force when performed in a quasi-static manner.

Moreover, these studies were conducted under *quasi-static* conditions. Bi-stable systems meanwhile can exhibit nonlinear *dynamic* behaviors like super-harmonic and chaotic responses. These non-linear dynamic characteristics can be exploited for shape morphing. Several relevant studies on bi-stable composites have demonstrated the feasibility of harnessing these rich dynamic characteristics for enhancing actuation authority[16,17]. In particular, dynamically exciting the bi-stable composite can trigger an intra-well resonance, resulting in snap-through and hence rapid shape morphing[16] with lower actuation levels compared to the quasi-static condition.

Therefore, the objective of this study is to demonstrate feasibility of using dynamic excitation to induce shape morphing (or folding) between the two stable states of water-bomb base shown in Figure 1(b-c). Via numerical simulations, we show that by harnessing the intra-well resonance of the water-bomb base structure, one can achieve rapid bi-directional morphing using relatively low actuation magnitude. The rest of this paper is organized as follows: In section 2, we define the dynamic problem of the morphing water-bomb base structure and derive the governing equation of motion. Section 3 discusses the numerical simulation results, and section 4 concludes this paper with summary and discussion.

2. DERIVING THE EQUATION OF MOTION

In this section, we derive the governing equation of motion of the water bomb base, which consists of six isosceles triangular facets connected along three valley and three mountain creases. We assume that the mechanism is symmetric and has one degree-of-freedom according to rigid-folding kinematics. The central vertex of the water-bomb pattern can move vertically, and the valley vertices can slide freely on an imaginary horizontal plane. Here, we choose the angle between vertical axis and valley creases (θ) as the independent variable (Figure 2(a)), so that we can derive the angles between the vertical axis and the mountain creases (γ in Figure 2(a)) as follows:

$$\gamma = \gamma_1 + \gamma_2 = \arccos\left[\frac{\cos\alpha}{\cos d/2}\right] + \arccos\left[\frac{\cos\theta}{\cos d/2}\right], \tag{1}$$

where $\alpha = \pi/3$ and d can be derived from:

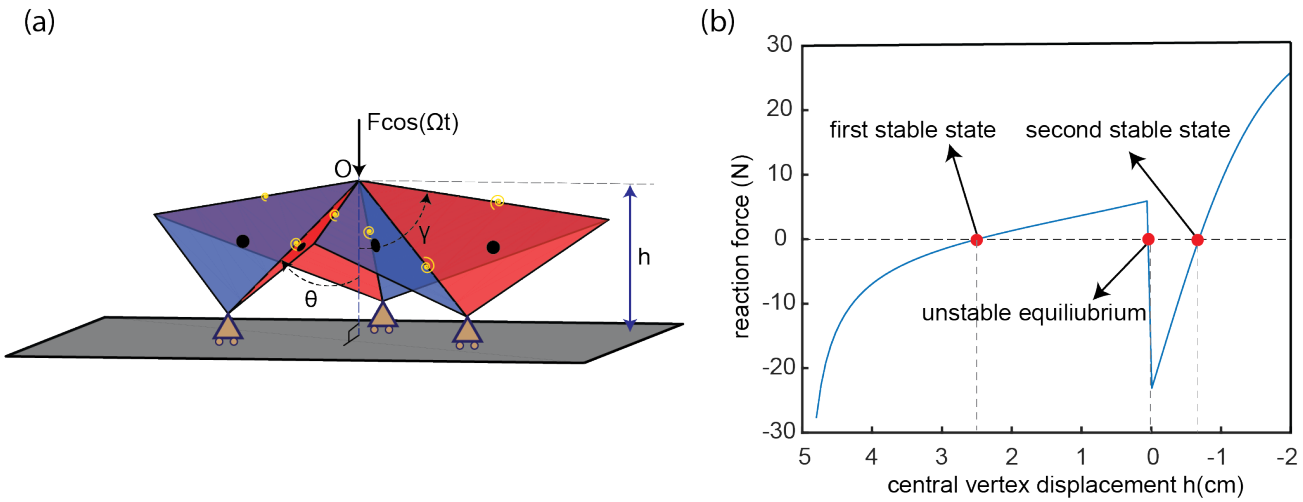

Figure 2. (a) Set-up of the dynamic analysis of water-bomb base mechanism. The three valley vertices are only allowed to slide freely on the horizontal plane. The yellow spirals show the torsional spring considered in the creases and the black dots demonstrate the centers of masses of each facet. (b) Reaction force-displacement curve of the water-bomb base mechanism due to the elastic deformation along the creases.

$$d = \arccos[\cos^2\theta + \sin^2\theta\cos\beta], \tag{2}$$

where $\beta = 2\alpha = 2\pi/3$. Furthermore, we can treat the central vertex of the water bomb base as a "moving origin", and describe the positions of the center of mass (CM) for every facet with respect to this origin as follows:

$$(\frac{2}{3}r\cos\alpha/2, \frac{(2i-1)\alpha}{2}, \frac{\theta+\gamma}{2}), \quad (i = 1,2,...,6), \tag{3}$$

2.1 Kinetic energy of the mechanism

As the water bomb base folds, its facets exhibit both translational and rotational motions with respect to the central vertex, therefore we can derive the absolute velocity of the center of mass of each facet as follows:

$$V_{CM} = V_O + V_{CM/O}. \tag{4}$$

where, V_O represents the absolute velocity of the central vertex and $V_{CM/O}$ is the relative velocity of the center of mass with respect to the central vertex (O). The position of the central vertex with respect to the imaginary horizontal plane can be described by $h = r\cos\theta$. Therefore, we can derive the velocity of the linear motion of the central vertex as follows:

$$\dot{h} = -r\dot{\theta}\sin\theta, \tag{5}$$

In addition, the center of mass of each facet will rotate around the central vertex with angular velocity $(\dot{\theta}+\dot{\gamma})/2$. Consequently, the magnitude of the absolute velocity of each center of mass (CM) can be written as:

$$|V_{CM}|^2 = \dot{h}^2 + \left(\frac{2}{3}r\cos\frac{\alpha}{2}\left(\frac{\dot{\theta}+\dot{\gamma}}{2}\right)\right)^2 - 2\dot{h}\left(\frac{2}{3}r\cos\frac{\alpha}{2}\left(\frac{\dot{\theta}+\dot{\gamma}}{2}\right)\right)\cos\left(\frac{\pi}{2}-\left(\frac{\theta+\gamma}{2}\right)\right). \tag{6}$$

Therefore, considering equation 5, the total kinetic energy of the system is:

$$T = 6\left(\frac{1}{2}m|V_{CM}|^2\right) = 3mr^2\dot{\theta}^2\sin^2\theta + 3m(\frac{2}{3}r\cos\frac{\alpha}{2})^2(\frac{\dot{\theta}+\dot{\gamma}}{2})^2 - 4mr^2\dot{\theta}\frac{\dot{\theta}+\dot{\gamma}}{2}\sin\theta\cos\frac{\alpha}{2}\sin(\frac{\theta+\lambda}{2}). \tag{7}$$

We can derive $\dot{\gamma}$ in terms of θ and $\dot{\theta}$. To this end, we need to write the equation 1 as:

$$\gamma = \arccos(I) + \arccos(II) =$$
$$\arccos[\frac{\cos\alpha}{\cos(\frac{1}{2}\arccos[\cos^2\theta+\sin^2\theta\cos\beta])}] + \arccos[\frac{\cos\theta}{\cos(\frac{1}{2}\arccos[\cos^2\theta+\sin^2\theta\cos\beta])}]. \tag{8}$$

Now, we can write $\dot{\theta}$ as:

$$\dot{\gamma} = [\frac{-I}{\sqrt{1-I^2}}] + [\frac{-II}{\sqrt{1-II^2}}]. \tag{9}$$

We can derive I as follows:

$$I = -\cos\alpha\times[\cos(\frac{1}{2}\arccos[\eta])]^{-2}\times\frac{-1}{2\sqrt{1-\eta^2}}\times\sin(\frac{1}{2}\arccos(\eta))\times(-2\dot{\theta}\cos\theta\sin\theta + 2\dot{\theta}\cos\theta\sin\theta\cos\beta), \tag{10}$$

where, $\eta = \cos^2\theta + \sin^2\theta\cos\beta$. We can also describe II as follows:

$$II = -\dot{\theta}\sin\theta\times[\cos(\frac{1}{2}\arccos[\eta])]^{-1} - \cos\theta\times[\cos(\frac{1}{2}\arccos[\eta])]^{-2}\times\sin(\frac{1}{2}\arccos\eta)\times\frac{-1}{2\sqrt{1-\eta^2}}$$
$$\times(-2\dot{\theta}\cos\theta\sin\theta + 2\dot{\theta}\cos\theta\sin\theta\cos\beta). \tag{11}$$

Therefore, we can describe equation 10 in terms of θ and $\dot{\theta}$. Hence, the relationship for the total kinetic energy can be fully described as a function θ and $\dot{\theta}$: $T(\theta,\dot{\theta})$.

2.2 Potential energies of the mechanism

Now we can focus on the potential energies of the water bomb base. We start with the gravitational potential energy. Considering the imaginary horizontal plane as the reference plane, we can write the vertical position of the centers of masses as:

$$Z_{CM} = r\cos\theta - \frac{2}{3}r\cos\frac{\alpha}{2}\cos\frac{\theta+\gamma}{2}. \tag{12}$$

Therefore, one can derive the gravitational potential energy of the system (V_G) as follows:

$$V_G = 6mgZ_{CM} = 6mg[r\cos\theta - \frac{2}{3}r\cos\frac{\alpha}{2}\cos\frac{\theta+\gamma}{2}]. \tag{13}$$

Again, we can describe γ in terms of θ (equation 1) and consequently we can derive the gravitational potential energy as a function of θ: $V_G(\theta)$. Now consider the elastic potential energy of the water bomb. Here we assume the isosceles triangular facets are rigid and the mountain and valley creases behave like spring hinges[18,19], so the spring energy stored along the creases can be calculated as:

$$V_E = \frac{3}{2}[k_{\gamma_m}(\gamma_m - \gamma_{m_0})^2 + k_{\gamma_v}(\gamma_v - \gamma_{v_0})^2], \tag{14}$$

where k_{γ_m} and k_{γ_v} are the effective torsional stiffness coefficients of the mountain and valley creases, respectively. γ_m and γ_v are the dihedral folding angles of the mountain and valley creases, respectively. In addition, γ_{m_0} and γ_{v_0} are the initial stress-free dihedral angles of the mountain and valley creases, respectively.

Using spherical trigonometry, one can derive the dihedral angles, i.e. γ_m and γ_v, in terms of θ, as follows[20]:

$$\gamma_m = -\pi + \arccos\left(1 + \frac{\cos^2\theta + \sin^2\theta\cos\beta - 1}{\sin^2\alpha}\right), \tag{15}$$

$$\gamma_v = \begin{cases} -\pi + 2\arccos\left(\cot\alpha\tan(\frac{1}{2}\arccos\eta)\right) + 2\arccos\left(\cot\theta\tan(\frac{1}{2}\arccos\eta)\right), (\theta \le \frac{\pi}{2}) \\ -\pi + 2\arccos\left(\frac{(\eta-1)\cot\theta}{\sin(\arccos\eta)}\right) + 2\arccos\left(\cot\alpha\tan(\frac{1}{2}\arccos\eta)\right), (\theta > \frac{\pi}{2}) \end{cases}. \tag{16}$$

Therefore, the elastic potential energy can be described as a function of θ: $V_E(\theta)$.

Measuring θ in a dynamic test can be a cumbersome task; therefore, we change the independent variable to the vertical displacement of the central vertex with respect to the horizontal plane *h* based on the following relation: $h = r\cos\theta$ (Figure 2(a)). Consequently, we can write the energies in terms of h and $\dot{h}$, using the following equations:

$$\theta = \arccos\frac{h}{r}, \tag{17}$$

$$\dot{\theta} = \frac{-\dot{h}}{r\sqrt{1-(\frac{h}{r})^2}}. \tag{18}$$

2.3 Lagrange equation

The Lagrangian of the system can be written as:

$$L = T(h,\dot{h}) - V_G(h) - V_E(h), \tag{19}$$

and can be used to derive the equation of motion as follows:

$$\frac{d}{dt}\frac{\partial L}{\partial \dot{h}} - \frac{\partial L}{\partial h} + c\frac{dh}{dt} = Fcos2\pi\omega t. \tag{20}$$

where F and ω are the amplitude and the frequency of vertical excitations at the central vertex, respectively and c is the linear damping coefficient of the system.

Using some mathematical manipulations, we can describe the equation of motion as:

$$\frac{d^2h}{dt^2} = \left(\frac{1}{2M}\right)\left(\left(F\cos 2\pi\omega t\right) - \left(2\frac{dM}{dt}\frac{dh}{dt}\right) + \left(\frac{dM}{dh}\left(\frac{dh}{dt}\right)^2\right) - \left(\frac{d(V_E)}{dh}\right) - \left(\frac{d(V_G)}{dh}\right) - \left(c\frac{dh}{dt}\right)\right), \tag{21}$$

where:

$$M = 3m + \left(\frac{3mr^2}{12}\right)\left[\frac{\frac{1}{r\delta_3} + \frac{3h^2\delta_2}{2r^3\delta_3{}^2\delta_1}}{\sqrt{1-\frac{h^2}{r^2\delta_3{}^2}}} + \frac{1}{r\sqrt{1-\frac{h^2}{r^2}}} + \frac{5h\delta_2}{4r^2\delta_3{}^2\delta_1\sqrt{1-\frac{1}{4\delta_3{}^2}}}\right]^2, \tag{22}$$

$$\frac{dM}{dh} = \left(\frac{3mr^2}{6}\right)\left(\frac{\sigma_2}{\sqrt{\sigma_4}} + \frac{1}{r\sqrt{\sigma_1}} + \frac{5\sigma_{10}h}{\sigma_3}\right)\times \tag{23}$$

$$\left(\begin{array}{l}\dfrac{9h^3}{4r^5\sigma_{12}(\sigma_{13}^2-1)}+\dfrac{3\sigma_{10}h}{\sigma_7}+\dfrac{9\sigma_{10}^2h^3}{2r^5\sigma_{12}^3(\sigma_{13}^2-1)}+\dfrac{9\sigma_{10}\sigma_{13}h^3}{2r^5\sigma_{12}^2\sigma_5}+\dfrac{h}{r^3\sigma_1^{3/2}}+\dfrac{\left(\dfrac{2h}{\sigma_9}-\dfrac{3\sigma_{10}h^3}{r^4\sigma_{12}^3\sigma_{11}}\right)\sigma_2}{2\sigma_4^{3/2}}+\\ \dfrac{15y^2}{8r^4\sigma_{12}(\sigma_{13}^2-1)\sqrt{\sigma_8}}+\dfrac{5\sigma_{10}}{\sigma_3}+\dfrac{\sigma_6}{4r^4\sigma_{12}^3(\sigma_{13}^2-1)\sqrt{\sigma_8}}+\dfrac{\sigma_6}{32r^4\sigma_{12}^5(\sigma_{13}^2-1)\sigma_8^{3/2}}+\dfrac{15\sigma_{10}\sigma_{13}h^2}{4r^4\sigma_{12}^2\sigma_5\sqrt{\sigma_8}}\end{array}\right),$$

$$\frac{dM}{dt}=\left(\frac{3mr^2}{6}\right)\left(\frac{\sigma_2}{\sqrt{\sigma_4}}+\frac{1}{r\sqrt{\sigma_1}}+\frac{5\sigma_{10}h}{\sigma_3}\right)\times$$

$$\left(\begin{array}{l}\dfrac{9h^3}{4r^5\sigma_{12}(\sigma_{13}^2-1)}+\dfrac{3\sigma_{10}h\dfrac{dh}{dt}}{\sigma_7}+\dfrac{9\sigma_{10}^2y^3\dfrac{dh}{dt}}{2r^5\sigma_{12}^3(\sigma_{13}^2-1)}+\dfrac{9\sigma_{10}\sigma_{13}h^3\dfrac{dh}{dt}}{2r^5\sigma_{12}^2\eta_1}+\dfrac{h\dfrac{dh}{dt}}{r^3\sigma_1^{3/2}}+\dfrac{\left(\dfrac{2h\dfrac{dh}{dt}}{\sigma_9}-\dfrac{3\sigma_{10}h^3\dfrac{dh}{dt}}{r^4\sigma_{12}^3\sigma_{11}}\right)\sigma_2}{2\eta_4^{3/2}}+\\ \dfrac{15h^2\dfrac{dh}{dt}}{8r^4\sigma_{12}(\sigma_{13}^2-1)\sqrt{\sigma_8}}+\dfrac{5\sigma_{10}\dfrac{dh}{dt}}{\sigma_3}+\dfrac{\eta_2}{4r^4\sigma_{12}^3(\sigma_{13}^2-1)\sqrt{\sigma_8}}+\dfrac{\eta_1}{32r^4\sigma_{12}^5(\sigma_{13}^2-1)\sigma_8^{3/2}}+\dfrac{15\sigma_{10}\sigma_{13}h^2\dfrac{dh}{dt}}{4r^4\sigma_{12}^2\eta_2\sqrt{\sigma_8}}\end{array}\right), \tag{24}$$

$$\frac{d(V_G)}{dh}=-6mg\left(\frac{1}{3}\left[2r\cos(\frac{\alpha}{2})\sin\left(\frac{\arccos(\frac{\cos(\alpha)}{\lambda_3})+\arccos(\frac{h}{r})+\arccos(\frac{h}{r\lambda_3})}{2}\right)\times\right.\right.$$
$$\left.\left.\left(\frac{\frac{1}{r\lambda_3}-\frac{\lambda_4\lambda_1h}{2r\lambda_3^2\lambda_2}}{2\sqrt{1-\frac{h^2}{r^2\sigma_3^2}}}+\frac{1}{2r\sqrt{1-\lambda_6}}-\frac{\lambda_1\lambda_4\cos(\alpha)}{4\lambda_3^2\lambda_2\sqrt{1-\frac{\cos^2(\alpha)}{\lambda_3^2}}}\right)\right]-1\right) \tag{25}$$

And finally,

$$\frac{d(V_E)}{dh}=\begin{cases}\frac{3}{2}\left[\begin{array}{l}\left(\frac{2k_m\mu_1\left(\pi+\gamma_{m_0}-\arccos(1-\mu_3)\right)}{\sin^2(\alpha)\sqrt{1-(\sigma_3-1)^2}}\right)+\\ 2k_v\left(\frac{2\left(\frac{\mu_2}{\mu_5}+\frac{\mu_2h^2}{r^3(1-\mu_7)^{3/2}}-\frac{\mu_1(\mu_2^2+1)h}{2r\mu_4\sqrt{1-\mu_7}}\right)}{\sqrt{\frac{\mu_2^2h^2}{r^2(\mu_7-1)}+1}}-\frac{\cot(\alpha)\mu_1(\mu_2^2+1)}{\mu_4\sqrt{1-\sigma_2^2\cot^2(\alpha)}}\right)\times\\ \left(\gamma_{v_0}+\pi-2\arccos(\mu_2\cot(\alpha))-2\arccos\left(\frac{\mu_2h}{\mu_5}\right)\right)\end{array}\right],(\theta\le\frac{\pi}{2})\\ \frac{3}{2}\left[\begin{array}{l}\left(\frac{2k_m\mu_1\left(\pi+\gamma_{m_0}-\arccos(1-\chi_3)\right)}{\sin^2(\alpha)\sqrt{1-(\chi_3-1)^2}}\right)+\\ 2k_v\left(\frac{2\left(\frac{\mu_6-\mu_7+1}{\chi_1}+\frac{(\mu_6-\mu_7+1)h^2}{r^3(1-\mu_7)^{3/2}\sqrt{\chi_1}}-\frac{\mu_1h}{\chi_1}+\frac{\mu_1(\mu_7-\mu_6)(\mu_6-\mu_7+1)h}{r\chi_4^{3/2}\sqrt{1-\mu_7}}\right)}{\sqrt{1-\frac{(\mu_6-\mu_7+1)^2h^2}{r^2(\mu_7-1)((\mu_7-\mu_6)^2-1)}}}-\right.\\ \left.\frac{\cot(\alpha)\mu_1(\mu_2^2+1)}{\mu_4\sqrt{1-\sigma_2^2\cot^2(\alpha)}}\right)\times\\ \left(\gamma_{v_0}+\pi-2\arccos(\chi_2\cot(\alpha))-2\arccos\left(\frac{(\mu_6-\mu_7+1)h}{\chi_1}\right)\right)\end{array}\right],(\theta>\frac{\pi}{2})\end{cases}\tag{26}$$

where: $\delta_1=\sqrt{1-\delta_4^2},\delta_2=\sin\left(\frac{\arccos(\delta_4)}{2}\right),\delta_3=\cos\left(\frac{\arccos(\delta_4)}{2}\right),\delta_4=\frac{3h^2}{2r^2}-\frac{1}{2}$. Furthermore, $\sigma_1=1-\frac{h^2}{r^2}$,

$\sigma_2=\frac{1}{r\sigma_{12}}+\frac{3\sigma_{10}y^2}{\sigma_7},\sigma_3=4r^2\sigma_{12}^2\sigma_{11}\sqrt{\sigma_8},\sigma_4=1-\frac{h^2}{\sigma_9},\sigma_5=(1-\sigma_{13}^2)^{3/2},\sigma_6=15\sigma_{10}^2,\sigma_7=2r^3\sigma_{12}^2\sigma_{11},\sigma_8=1-\frac{1}{4\sigma_{12}^2}$,

$\sigma_9=r^2\sigma_{12}^2,\sigma_{10}=\sin\left(\frac{\arccos(\sigma_{13})}{2}\right),\sigma_{11}=\sqrt{1-\sigma_{13}^2},\sigma_{12}=\cos(\frac{\arccos(\sigma_{13})}{2}),\sigma_{13}=\frac{3h^2}{2r^2}-\frac{1}{2}$. Also, $\eta_1=(1-\sigma_{13}^2)^{3/2}$ and

$\eta_2=15\sigma_{10}^2h^2\frac{dh}{dt}$. In addition, $\lambda_1=\frac{2h}{r^2}-\frac{2h\cos(\beta)}{r^2},\lambda_2=\sqrt{1-\lambda_5^2},\lambda_3=\cos\left(\frac{\arccos(\lambda_5)}{2}\right),\lambda_4=\sin\left(\frac{\arccos(\lambda_5)}{2}\right)$,

$\lambda_6=\frac{h^2}{r^2}$. And finally, $\lambda_5=\lambda_6-\cos(\beta)(\lambda_6-1),\mu_1=\frac{2h}{r^2}-\frac{2\cos(\beta)h}{r^2},\mu_2=\tan\left(\frac{a\cos(\mu_7-\mu_6)}{2}\right),\mu_3=\frac{\mu_6-\mu_7+1}{\sin^2(\alpha)}$,

$\mu_4=\sqrt{1-(\mu_7-\mu_6)^2},\mu_5=r\sqrt{1-\mu_7},\mu_6=(\mu_7-1)\cos(\beta),\mu_7=\frac{h^2}{r^2},\chi_1=r\sqrt{(1-\mu_7)\chi_4},\chi_2=\tan\left(\frac{\arccos(\mu_7-\mu_6)}{2}\right)$

$$\chi_3 = \frac{\mu_6 - \mu_7 + 1}{\sin^2(\alpha)}, \chi_4 = 1 - (\mu_7 - \mu_6)^2.$$

3. NUMERICAL SIMULATIONS

Now that we have the equation of motion of the water-bomb base system (equation 21), we solve it numerically using MATLAB ODE45 and perform a stroboscopic sampling to determine the intra-well resonance frequencies of the mechanism near its two stable equilibria. The results are presented in Figure 3(a, b) and the values of physical parameters considered for the numerical simulations are listed in Table 1.

Figure 2(b) demonstrates the reaction force-displacement curve of the mechanism with its stable and unstable equilibria. One can clearly notice that the water-bomb base possesses an inherently asymmetric force-displacement curve, so that its tangent stiffness are notably different near the two stable equilibria. This explains the difference between the intra-well resonance frequencies of the water bomb base at the first and second stable states (Figure 3(a, b)).

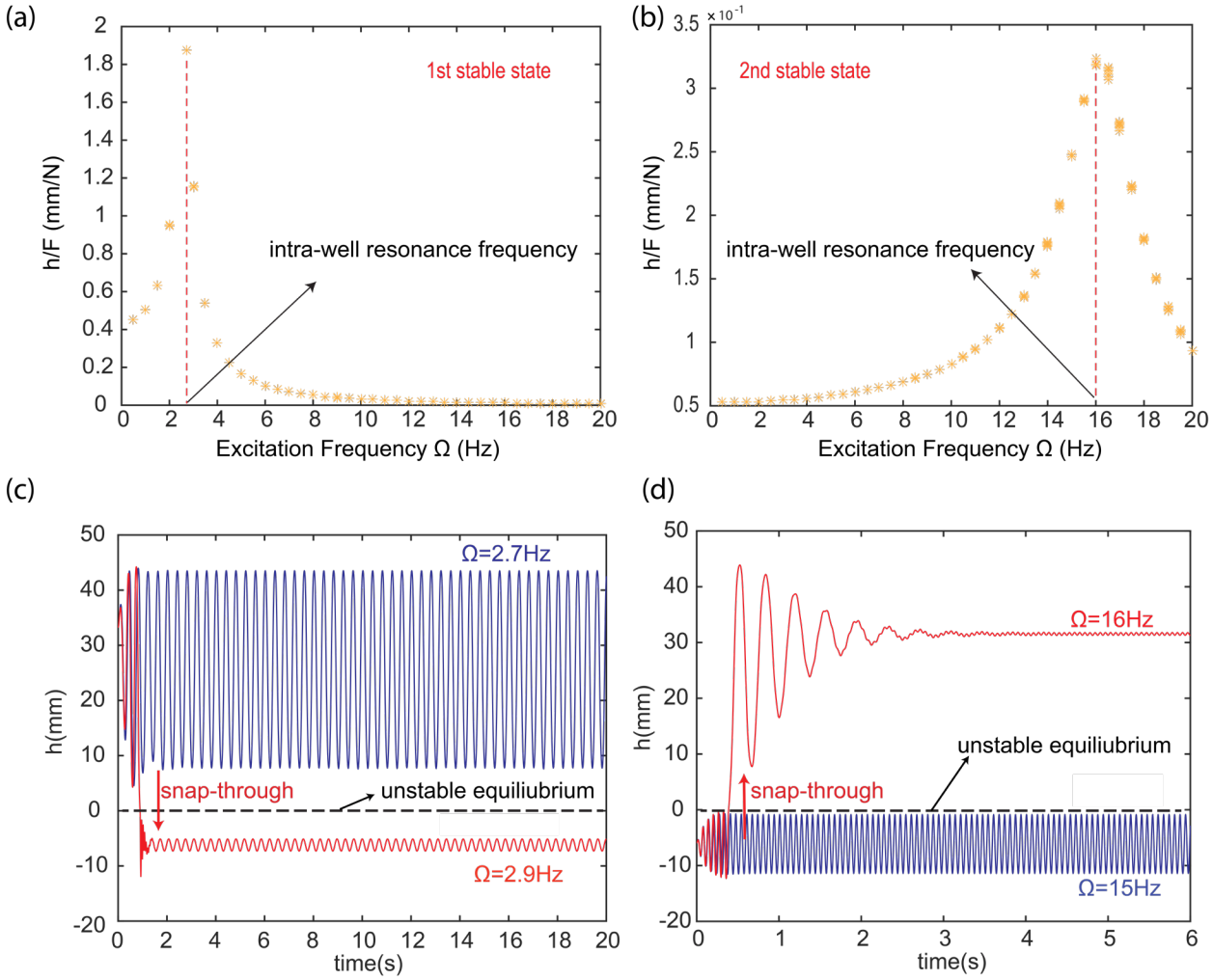

Figure 3. Stroboscopic sampling results for intra-well oscillations near the (a) 1st stable state and (b) 2nd stable state. (c) The idea of triggering the intra-well resonance frequencies for the (c) 1st stable state and (d) 2nd stable state. F=2N in (c) and (d). The blue and red curves show the response of the water-bomb mechanism when excited at non-resonance and resonance frequencies, respectively.

Table 1. Physical parameters considered for the stroboscopic sampling.

θ_0	F	r (crease length)	m (each facet)	$k_m = k_v$	g
$\pi/4$	1N	5cm	0.03kg	0.05 Nm/rad	9.8 m/s^2

Now that we know the resonance frequencies of the structure at both stable states, we can investigate the effect of targeting at those frequencies. Figure 3(c) shows the numerical simulation results based on the parameters of Table 1 except for F, which is set to $2N$. If the water bomb base is settled at its first stable state initially, one can excite it using the corresponding intra-well resonance frequency at 2.9Hz and trigger a rapid "jump" (or snap-through) to the second stable state. Moreover, once the jump occurs, the water bomb will remain oscillating near the second state with a small amplitude. The opposite jump from the second to first stable state is also feasible if the excitation frequency is changed to the second intra-well resonance frequency at 16Hz (Figure 3(d)).

In Figure 3(c), we can observe that to reach the second stable state, it is only sufficient to pass the unstable equilibrium. This is achieved by exciting the mechanism with a relatively small force at the resonance frequency ($F = 2N$ compared to $F = 6N$ for the quasi-static loading (Figure 2(b))). Such an advantage in small excitation magnitude is even more significant in the reverse jump form the second stable state to the first one (Figure 3(d)), where the dynamic excitation amplitude ($F = 2N$) is much smaller than the quasi-static force needed ($F = 24N$) observed in Figure 2(b).

These results discussed in this study are just for a specific case study, however, the same principle holds true for any other water-bomb base designs. In addition, one can tailor the number of creases or change the creases stiffness to acquire a desired *difference* in the resonance frequencies, or tune the energy bandgaps[21] to achieve a specific dynamic morphing behavior.

4. DISCUSSION AND CONCLUSION

In this study, we introduce the idea of utilizing intra-well oscillations of a bi-stable water-bomb base origami to achieve bi-directional and rapid shape morphing. For the first time, we derive the dynamic equation of motion and solve it numerically to obtain the different intra-well resonance frequencies of the origami structure at its first and second stable states. We observe that such a difference in resonance frequencies stems from an inherent asymmetry of the structure with respect to its unstable (flat-state) equilibrium, and it can be harnessed for an advantageous and efficient morphing. It is shown that utilizing the resonance frequencies for dynamic snap-through can increase the external actuation authority, and enables us to achieve shape morphing via folding with relatively low excitation levels. Furthermore, the inherent bi-stability of the mechanism provides a powerful foundation for stabilizing and maintaining the structure at a desired configuration without the need for constant external power supply.

It is also worth noting that although this study assumed on an external actuation, the underlying principles are still valid if the actuators are embedded and internal. Therefore, the outcome of this research may lead to the emergence of a novel category of origami-based morphing and smart structures with desired dynamic characteristics.

5. ACKNOWLEDGEMENT

The authors acknowledge the support by the National Science Foundation (Award # CMMI-1633952, 1751449 CAREER, 1760943) and Clemson University (via startup funding and Dean's faculty fellow award).

REFERENCES

[1] Kuder, I. K., Arrieta, A. F., Raither, W. E. and Ermanni, P., "Variable stiffness material and structural concepts for morphing applications," Prog. Aerosp. Sci. **63**, 33–55 (2013).

[2] Barbarino, S., Bilgen, O., Ajaj, R. M., Friswell, M. I. and Inman, D. J., "A review of morphing aircraft," J. Intell. Mater. Syst. Struct. **22**(9), 823–877 (2011).

[3] Schioler, T. and Pellegrino, S., "Space Frames with Multiple Stable Configurations," AIAA J. **45**(7), 1740–1747 (2007).

[4] Abdulrahim, M. and Lind, R., "Using Avian Morphology to Enhance Aircraft Maneuverability," AIAA Atmos. Flight Mech. Conf. Exhib., American Institute of Aeronautics and Astronautics, Reston, Virigina (2006).

[5] Lachenal, X., Daynes, S. and Weaver, P. M., "Review of morphing concepts and materials for wind turbine blade applications," Wind Energy **16**(2), 283–307 (2013).

[6] Li, S., Fang, H., Sadeghi, S., Bhovad, P. and Wang, K.-W., "Architected Origami Materials: How Folding Creates Sophisticated Mechanical Properties," Adv. Mater. **1805282**, 1805282 (2018).

[7] Schenk, M. and Guest, S. D., "Geometry of Miura-folded metamaterials," Proc. Natl. Acad. Sci. **110**(9), 3276–3281 (2013).

[8] Fang, H., Li, S. and Wang, K. W., "Self-locking degree-4 vertex origami structures," Proc. R. Soc. A Math. Phys. Eng. Sci. **472**(2195), 20160682 (2016).

[9] Fang, H., Li, S., Ji, H. and Wang, K. W., "Dynamics of a bistable Miura-origami structure," Phys. Rev. E **95**(5), 52211 (2017).

[10] Sadeghi, S. and Li, S., "Harnessing the Quasi-Zero Stiffness From Fluidic Origami for Low Frequency Vibration Isolation," Vol. 2 Model. Simul. Control Adapt. Syst. Integr. Syst. Des. Implementation; Struct. Heal. Monit., V002T03A008, ASME (2017).

[11] Crivaro, A., Sheridan, R., Frecker, M., Simpson, T. W. and Von Lockette, P., "Bistable compliant mechanism using magneto active elastomer actuation," J. Intell. Mater. Syst. Struct. **27**(15), 2049–2061 (2016).

[12] Ahmed, S., Ounaies, Z. and Frecker, M., "Investigating the performance and properties of dielectric elastomer actuators as a potential means to actuate origami structures," Smart Mater. Struct. **23**(9) (2014).

[13] Peraza-Hernandez, E., Hartl, D. and Malak, R., "Simulation-Based Design of a Self-Folding Smart Material System," Vol. 6B 37th Mech. Robot. Conf., V06BT07A045, ASME (2013).

[14] Hanna, B. H., Lund, J. M., Lang, R. J., Magleby, S. P. and Howell, L. L., "Waterbomb base: a symmetric single-vertex bistable origami mechanism," Smart Mater. Struct. **23**(9), 94009 (2014).

[15] Bowen, L., Springsteen, K., Feldstein, H., Frecker, M., Simpson, T. W. and von Lockette, P., "Development and Validation of a Dynamic Model of Magneto-Active Elastomer Actuation of the Origami Waterbomb Base," J. Mech. Robot. **7**(1), 11010 (2015).

[16] Arrieta, A. F., Bilgen, O., Friswell, M. I. and Hagedorn, P., "Dynamic control for morphing of bi-stable composites," J. Intell. Mater. Syst. Struct. **24**(3), 266–273 (2013).

[17] Senba, A., Ikeda, T. and Ueda, T., "A Two-Way Morphing Actuation of Bi-Stable Composites with Piezoelectric Fibers," 51st AIAA/ASME/ASCE/AHS/ASC Struct. Struct. Dyn. Mater. Conf. 18th AIAA/ASME/AHS Adapt. Struct. Conf. 12th(August 2015) (2010).

[18] Fang, H., Li, S., Ji, H. and Wang, K. W., "Uncovering the deformation mechanisms of origami metamaterials by introducing generic degree-four vertices," Phys. Rev. E **94**(4), 43002 (2016).

[19] Waitukaitis, S., Menaut, R., Chen, B. G. and van Hecke, M., "Origami Multistability: From Single Vertices to Metasheets," Phys. Rev. Lett. **114**(5), 55503 (2015).

[20] Hanna, B. H., Lund, J. M., Lang, R. J., Magleby, S. P. and Howell, L. L., "Waterbomb base: a symmetric single-vertex bistable origami mechanism," Smart Mater. Struct. **23**(9), 94009 (2014).

[21] Hanna, B. H., Magleby, S. P., Lang, R. J. and Howell, L. L., "Force–Deflection Modeling for Generalized Origami Waterbomb-Base Mechanisms," J. Appl. Mech. **82**(8), 81001 (2015).